Available online at www.sciencedirect.com
SCIENCE DIRECT®
C. R. Physique 4 (2003) 1175–1185
COMPTES RENDUS PHYSIQUE

IR vision: from chip to image/Vision IR : du composant à l'image

New techniques of characterisation

Nicolas Guérineau *, Sylvain Rommeluere, Emmanuel Di Mambro, Isabelle Ribet, Jérôme Primot

ONERA, chemin de la Hunière, 91761 Palaiseau cedex, France

Presented by Guy Laval

Abstract

During the last decade, amazing advances in microelectronics have led to the development of large infrared focal plane arrays (IRFPAs) with a high density of pixels per square centimetre. Bispectral and soon multispectral detectors are now under development. In order to follow or even anticipate this race for spatial and spectral resolution, new techniques of characterisation have been developed in our laboratory, allowing the measurement of the spatial and spectral responses of a hundred of thousands pixels forming the IRFPA. Thus, a test bench for the measurement of hyperspectral cartographies has been realised. The principle of measurement and experimental results will be presented. For the measurement of spatial responses, the projection of targets that illuminate the entire surface of the IRFPA and contain sub-pixel details is required in order to extract the line (or spot) spread function of every pixel. For this, non-imaging techniques of projection based on the self-imaging property of periodic targets have been elaborated. The first results and the potential of this original approach will be discussed. ***To cite this article: N. Guérineau et al., C. R. Physique 4 (2003).***

Résumé

Des techniques nouvelles de caractérisation. Les progrès fulgurants en microtechnologie durant la dernière décennie ont abouti à la réalisation de plans focaux infrarouge (PFI) de grand format, intégrant une importante densité de détecteurs au centimètre carré. Prochainement, les grands plans focaux bispectraux ou multispectraux verront le jour. Pour suivre voire anticiper cette course à la résolution spatiale et spectrale, le laboratoire de caractérisation des détecteurs de l'Onéra a développé de nouvelles techniques de mesures permettant d'extraire les réponses spatiales et spectrales des centaines de milliers de pixels formant le PFI. Ainsi, un banc de mesure de cartographies hyperspectrales a été mis au point, dont le principe de mesure sera présenté. On montrera des exemples de mesures obtenues avec ce banc de test et les paramètres utiles que l'on peut en extraire. Pour les caractérisations en réponse spatiale, la projection de mires couvrant toute la surface du PFI et contenant des détails sub-pixels est nécessaire pour extraire les fonctions d'étalement de chaque détecteur élémentaire. Pour cela, des techniques de projection sans optiques, reposant sur les propriétés auto-imageantes de mires périodiques ont été élaborées. Les premiers résultats obtenus et les potentialités de cette approche originale seront discutés. ***Pour citer cet article : N. Guérineau et al., C. R. Physique 4 (2003).***

Keywords: Infrared focal plane arrays; Metrology; Spectrometry; MTF; Talbot

Mots-clés : Plans focaux infrarouge ; Métrologie ; Spectrométrie ; FTM ; Talbot

* Corresponding author.
E-mail address: nicolas.guerineau@onera.fr (N. Guérineau).

1631-0705/$ – see front matter
doi:10.1016/j.crhy.2003.10.019

1. Introduction

Motivated by increasing requirements for high-performance infrared systems in terms of spatial and spectral resolution, much research in infrared detector technology and microelectronics has led to the development of large focal plane arrays with a high number of small pixels and with customised spectral responses. For the technologist, an intimate understanding of the diffraction and interference phenomena in the pixel is necessary in order to reach this ultimate performance. For the design engineer, the focal plane array is the key element of his infrared system and the detector's spectral and spatial filtering effects have to be precisely calibrated.

To fulfil these emerging requirements, accurate optical characterisations are necessary. Unfortunately, finding adequate test equipment in this area becomes a challenge [1]. That is why our laboratory has explored new techniques of characterisation. In Section 2, a technique for measuring the spectral responses of an IRFPA is presented and an example of its characterisation is given. For the measurement of the spatial responses, our laboratory has developed an original technique based on the projection of self-imaging patterns. The first results and the potential of this original approach are discussed in Section 3.

2. Measurement of spectral responses

This section presents the technique developed at Onera for measuring the spectral responses of IRFPAs. After a brief review of the existing test equipment, our technique is detailed and an example of characterisation is then proposed.

2.1. Definition and state of the art

As a general definition, the spectral response $R(\lambda)$ of a detector is obtained by comparing the signal from the detector to the signal from a reference detector as a function of the wavelength of the incident radiation. A direct way to measure this function is to use a blackbody source, a modulator and a monochromator or a spectral filter. Historically, this technique has been developed for the characterisation of elementary detectors with their electronics consisting of a preamplifier, amplifier and a spectrum analyser [2].

An indirect way to measure $R(\lambda)$ is to use a Fourier Transform infrared (FTIR) spectrometer. The general principle is to measure the response of the detector to a temporally-varying signal called an interferogram. If a single wavelength of light is present, this interferogram will be a single sinusoid of period proportional to the wavelength and the detector will deliver a sinusoidal signal whose modulation, compared to the modulation of a reference signal, is the spectral response $R(\lambda)$.

These two general approaches for measuring the spectral responses are illustrated in Fig. 1.

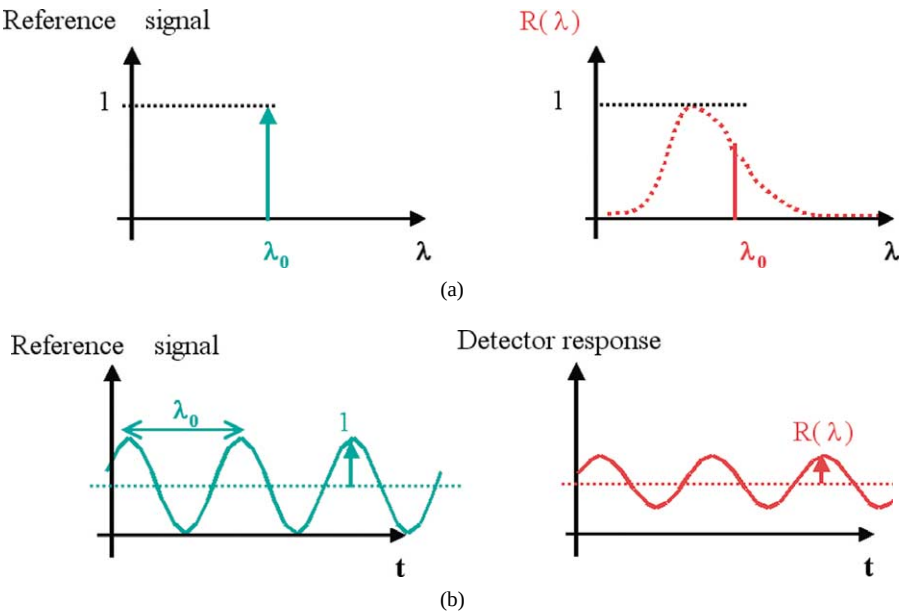

Fig. 1. General approaches for determining the spectral response: (a) direct; and (b) indirect methods.

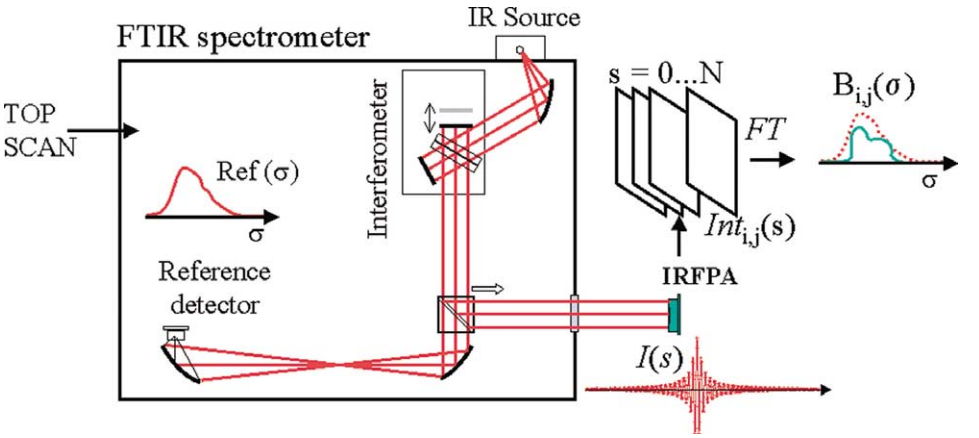

Fig. 2. Onera test equipment for the measurement of IRFPAs hyperspectral cartographies. Experimental set-up.

Based on these approaches, test instruments can be obtained from various commercial suppliers. From our point of view, the FTIR spectrometer is nowadays the solution preferred by industrial and research laboratories to make spectral measurements of infrared detectors. Several reasons can explain this. On a theoretical level, FTIR spectrometers have several known advantages over monochromators, in terms of throughput (Jacquinot advantage) and signal-to-noise ratio (Fellgett advantage) [3]. On a practical level, a FTIR instrument can deliver measurements of high resolution, in a few seconds, on a large spectral range (from typically 1.5 μm to 20 μm) whereas an instrument based on a grating monochromator requires much more time (typically 30 minutes) and at least one replacement of the dispersive element (grating) in order to explore that spectral range.

2.2. Technique developed at Onera

The technique developed at Onera is based on the use of a commercial FTIR spectrometer. The originality of this test bench is that all the pixels of an IRFPA are tested simultaneously, leading to the spectral responses $R_{i,j}(\lambda)$ of each pixel (i, j) on a wide spectral range and with a high resolution.

Fig. 2 shows the instrument layout. A Fourier-Transform spectrometer (Bruker, Equinox IFS55) is used to produce either a reference spectrum $Ref(\sigma)$ (where $\sigma = 1/\lambda$ is the wavenumber) delivered by an internal reference detector, or an external collimated beam of uniform intensity $I(s)$, function of a scanning parameter s directly linked to the position of the movable mirror of the interferometer. This movable mirror is held stationary at each sampling for several hundreds of milliseconds. During this time, an image $Int_{i,j}(s)$ of this uniform beam is grabbed and the operation is repeated for several thousands of s. For each pixel (i, j), the Fourier Transform of the interferogram $Int_{i,j}(s)$ is computed, leading to a spectrum $B_{i,j}(\sigma)$ equal to the reference light spectrum $Ref(\sigma)$ multiplied by the searched spectral response $R_{i,j}(\sigma)$. At a given wavenumber σ, we obtain an array of responses that we call the hyperspectral cartography of responses at wavelength $\lambda = 1/\sigma$.

2.3. Example of hyperspectral cartographies

Tests have been performed on a large format (640 × 512) IRFPA of quantum-well technology operating in the 8–10 μm spectral range. We have chosen this example because the prototype tested had several small defects that produce spectacular hyperspectral cartographies. For this technology, the phenomena of diffraction and interference are expected to have a strong impact on the spectral responses due to the structure of the pixel [4].

On a practical level, 6575 images have been grabbed leading to the measurement of spectral responses $R_{i,j}(\nu)$ with a resolution of 4 cm^{-1} (that is ∼30 nm around 8.5 μm). The spectral curves correspond to a quasi plane-wave illumination at normal incidence, the light source being viewed at an angle of 5°. Fig. 3 shows examples of measurements produced by the test bench. At a given wavelength, a cartography of the pixels responses can be obtained, as illustrated in Fig. 3(a). This cartography shows that the pixels on the corners of the sensor are not characterised. This shadow effect is due to the cold shield, placed in front of the sensor and illuminated by a collimated beam in quasi normal incidence. Several effects can be noticed on this cartography: a grid structure appears explained by a periodic positioning of the grating in the pixel. On the lower part of the cartography, Fizeau fringes appear explained by a residual gradient of substrate (GaAs) thickness. For a given pixel (i, j), its spectral response $R(\lambda)$ can be graphed, as illustrated in Fig. 3(b). These hyperspectral measurements of a hundred of thousand pixels produce a wealth of information that make it possible to quantify the physical phenomena of diffraction and interference involved in the pixels and to adjust rigorous models developed by the technologists [5].

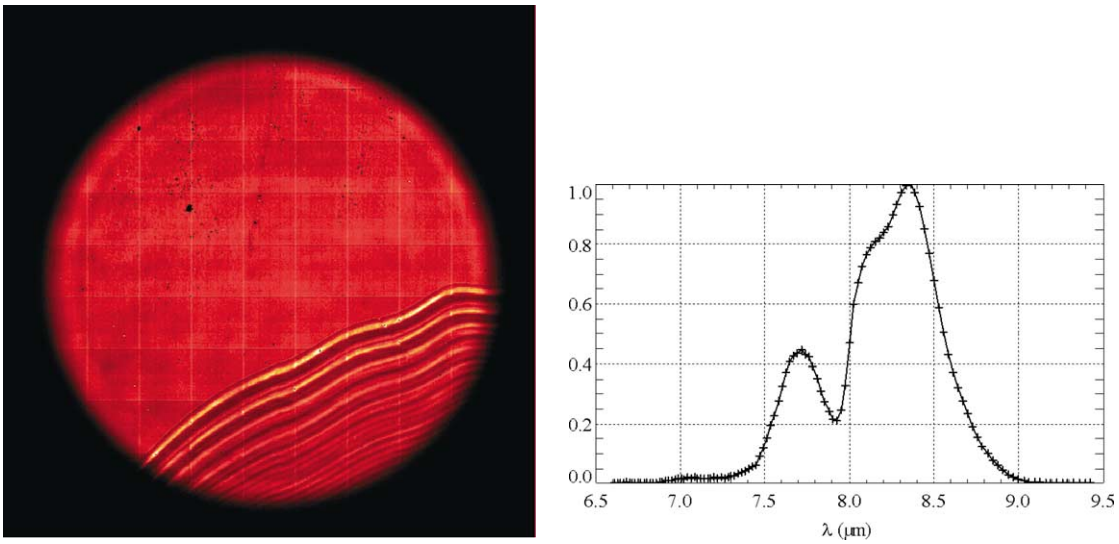

(a) (b)

Fig. 3. Experimental results obtained on a 640 × 512 IRFPA of quantum-well technology; (a) example of hyperspectral cartography at $\lambda = 8.36$ μm (512 by 512 pixels are represented); (b) example of spectral response of a pixel (i, j).

3. Measurement of spatial responses

This section presents the technique developed at Onera for measuring the spatial responses of IRFPAs. After a brief review of the existing test equipment, our technique is detailed and examples of characterisation are then presented.

3.1. Definition and state of the art

By definition, the spatial response of a pixel, also called the point spread function, $PSF(x, y)$, is obtained by measuring the response of the detector as a function of the position (x, y) of an ideal point source in the detector plane. This curve gives to the technologist useful information on the pixel's sensitive area and quantifies possible phenomena of diffusion and diffraction inside the pixel or between two adjacent pixels (crosstalk). Instead of a point source, an ideal line source can be scanned across the detector to find the pixel's line spread function (LSF). The Fourier transform of the LSF results in the optical transfer function (OTF), the modulus of which is the modulation transfer function (MTF). The MTF describes the spatial filtering effects of the pixel, which are a major contributor in the final infrared system's ability to reproduce faithfully the spatial-frequency content of a scene.

A direct way to measure the LSF (or PSF) is to perform a line (or spot) scan (see [1, pp. 223–232]). Test benches based on this principle require high-aperture optics and high-precision mechanical devices to project and scan a thin line (or spot). Even with excellent optics, the line (or spot) projected has a finite size due to the diffraction limit that has to be deconvolved from the measure. This procedure of deconvolution is a critical point that requires one to predict and control correctly the profile of the detail projected. In the IR spectral range these constraints are critical since the sensor is included in a cryogenic assembly where no moving parts can be used.

In addition, this local test is heavy to perform for the characterisation of large infrared focal arrays. A connected approach is to perform a static line scan by creating a periodic array of lines (or spots), each line illuminating a pixel at a specific sub-pixel location. Assuming that all the pixels have the same LSF, this function can then be reconstructed by overlaying the various responses according to its line- (or point-) source location [6].

An indirect and non-local way to measure the LSF is to estimate directly the MTF. The general principle is to project periodic patterns (ideally a sinusoidal intensity-profile) and to extract from the image delivered by the FPA the sinusoid whose modulation as a function of the input spatial-frequency gives the MTF [7]. This Fourier-transform approach is rarely used in industrial laboratories to test IRFPAs for several reasons. First, sin intensity patterns of varying spatial frequency and controlled contrast are difficult to create. Second, one must properly account for the aliasing effects that appear when we want to explore the MTF beyond the Nyquist frequency. However, we have developed an original approach of this Fourier-transform technique that overrides these difficulties.

3.2. Technique developed at Onera

The technique we have developed is based on the Fourier-transform approach. The principle is to project a periodic intensity pattern onto the IRFPA and to compute OTF values from a single image by extracting the spatial frequencies excited by this pattern. More precisely, during image acquisition the input spatial-frequency spectrum is multiplied by the pixel OTF and replicated in the two sampling directions at the sampling frequency. This replication can generate well-known aliasing effects that can disturb the measure if no care is taken. To avoid these effects, a solution is to choose a period d of the projected pattern nonmultiple of the sampling pitch. In this way, the spatial frequencies beyond the Nyquist frequency are folded on spatial frequencies of null amplitude [8]. This method has been extended to a 1D periodic target that is canted with respect to the pixel grid. This way, no conditions are required for d [9].

Another originality of the technique lies in the projection system that exploits the self-imaging property of gratings, called the Talbot effect [10]. When a thin periodic object is illuminated by a monochromatic plane wave propagating in a given direction, a series of images, called self-images, are formed at regular distances in this direction at a longitudinal period of $2d^2/\lambda$, where d is the object period and λ is the wavelength of light. This property is illustrated in Fig. 4.

By positioning the IRFPA in one of these planes, one obtains the formation of numerous thin lines without any optics. After a first experiment of validation, [11] a test bench has been developed.

3.3. First test bench based on the Talbot effect

Fig. 5 shows the layout of the instrument. The sensor is included in a specific Dewar where the target is also mounted. Behind the target, a cold filter and a cold radiation shield minimise background flux. We can notice that from the exit pupil of the collimator to the back surface of the target, useful flux is propagated by a plane wave, so that no geometrical aberrations are introduced by the window of the cryostat and the cold filter. Moreover, as the projecting system is shift-invariant along the direction of the target lines, a slit-type source with the slit parallel to the target lines is used to increase the useful flux. Outside the cryostat, an interferential filter is used to produce a quasi-monochromatic light.

As no moving parts can be implemented in the cryostat, the mechanical distance z between the IRFPA and the target is constant. For a given working wavelength λ_0 and a target period d, this value is near half of the Talbot distance d^2/λ_0. In this plane, the original intensity pattern is reproduced but shifted by half of a grating period d. However, like other projecting

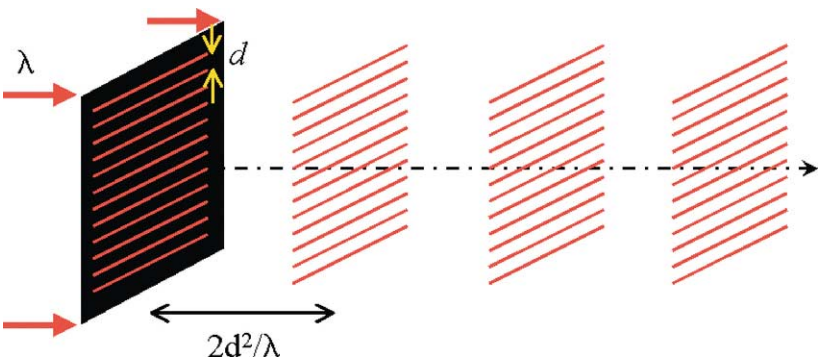

Fig. 4. Self-imaging property of gratings (Talbot effect), illustration.

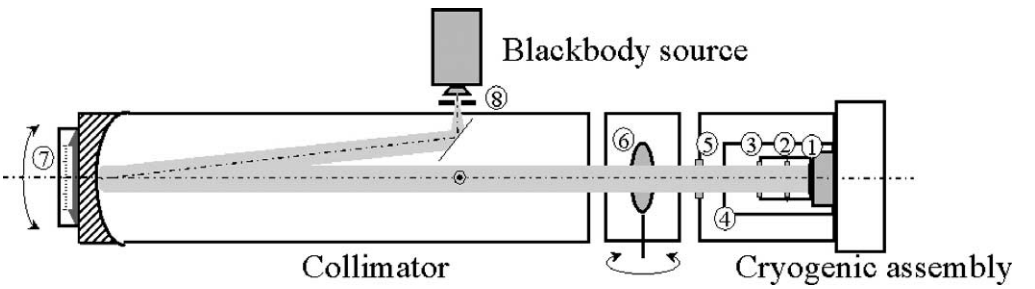

Fig. 5. Talbot test bench. 1: tested sensor, 2: periodic target, 3: cold filter, 4: cold shield, 5: window, 6: rotating interferential filter, 7: translation stage, 8: slit (parallel to the target slits).

systems, precise focusing is needed. The focusing here consists in adjusting the focal distance d^2/λ_0 to the mechanical distance z. This function is provided by the interferential filter. By tilting this filter, we can tune the peak passband wavelength λ_0 precisely.

The test bench offers two different types of measurements.

Firstly, local LSF assessments can be made. As shown in Fig. 5, the collimator used can be slightly tilted. This motion is controlled with a translation stage located under the back of the collimator, near the primary mirror. The collimator can then revolve on a vertical axis that cuts across the optical axis near the small plane mirror, at a distance of about 700 mm from the primary mirror. The translation stage has a resolution of 0.1 mm. This resolution corresponds to an angular resolution of about 0.15 mrad; such a tilt angle of the incident plane wave on the target leads to a translation resolution of the projected pattern of 1 µm. This property has been exploited to explore the intensity profile of the projected lines, using a reference detector with a very small sensitive area (5 µm). The target was a silicon window with a chromium mask of 200 slits 17 µm wide and spaced 155 µm apart. The chromium side faces the sensor at a distance of ∼7 mm, corresponding to half of the Talbot distance. An example of experimental profile is depicted in Fig. 6. The profile obtained exhibits a width of 12 µm at 50% and the shape of this profile has been correctly predicted by our model [12].

After calibrating our projection system, LSF assessments have been made on a 256 × 256 MCT sensor designed for the 3–5 µm spectral range with a 35 µm pitch. The effective sensitive area of the pixel was 25 µm. By translating the projected thin slits in the sensor plane of at least one period, all the pixels of the FPA can be line scanned simultaneously, leading to the computation of the 65 000 LSFs [13]. Statistics from these measurements can be made. As an example, an histogram of the LSF widths has been computed and is plotted in Fig. 7. We observe that the mean width is 20.0 µm and the standard deviation of this parameter across the FPA is 0.3 µm.

The test bench allows a second type of LSF assessment. Apart from one image recorded, a mean LSF can be computed using our Fourier transform approach. This approach is illustrated in Fig. 8. From a recorded image, Fig. 8(a), the discrete spatial frequencies excited by the periodic pattern projected are extracted by computing its 2D discrete Fourier transform, Fig. 8(b). These Fourier coefficients (c) $D_{p,\mathrm{out}}$ correspond to the predicted Fourier coefficients of the projected pattern, $D_{p,\mathrm{in}}$, multiplied by the searched OTF at these discrete frequencies, Fig. 8(d). Then an inverse Fourier transform of this OTF yields the mean LSF of the pixels, Fig. 8(e).

3.4. Discussion

The study made with this first test bench has demonstrated the advantage of using periodic targets to measure accurately the spatial responses of an IRFPA of small pixels (∼25 µm) operating in the 3–5 µm spectral range. For the characterisation of IRFPAs in the 8–12 µm spectral range, fundamental limitations are predicted by our model based on a nonparaxial description of the Talbot effect.

3.4.1. Fundamental limitations of the monochromatic Talbot effect

To explain the origin of these nonparaxial effects, let us consider the scheme of Fig. 9. When illuminated by a plane monochromatic wave, the grating diffracts a large angular spectrum of plane waves corresponding to the diffraction orders.

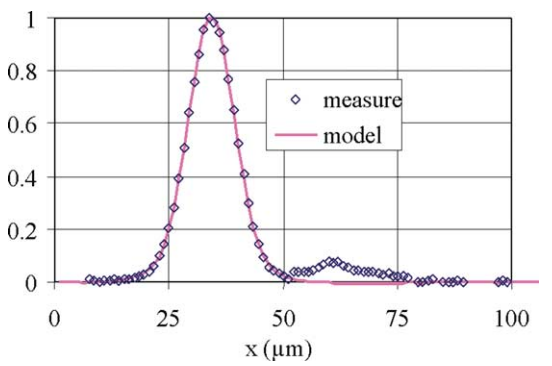

Fig. 6. Experimental and predicted profiles of the projected lines in the detection plane.

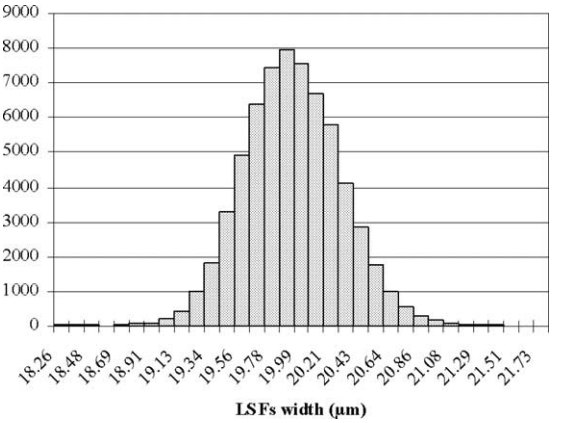

Fig. 7. Histogram of the widths of the 65 000 LSFs measured.

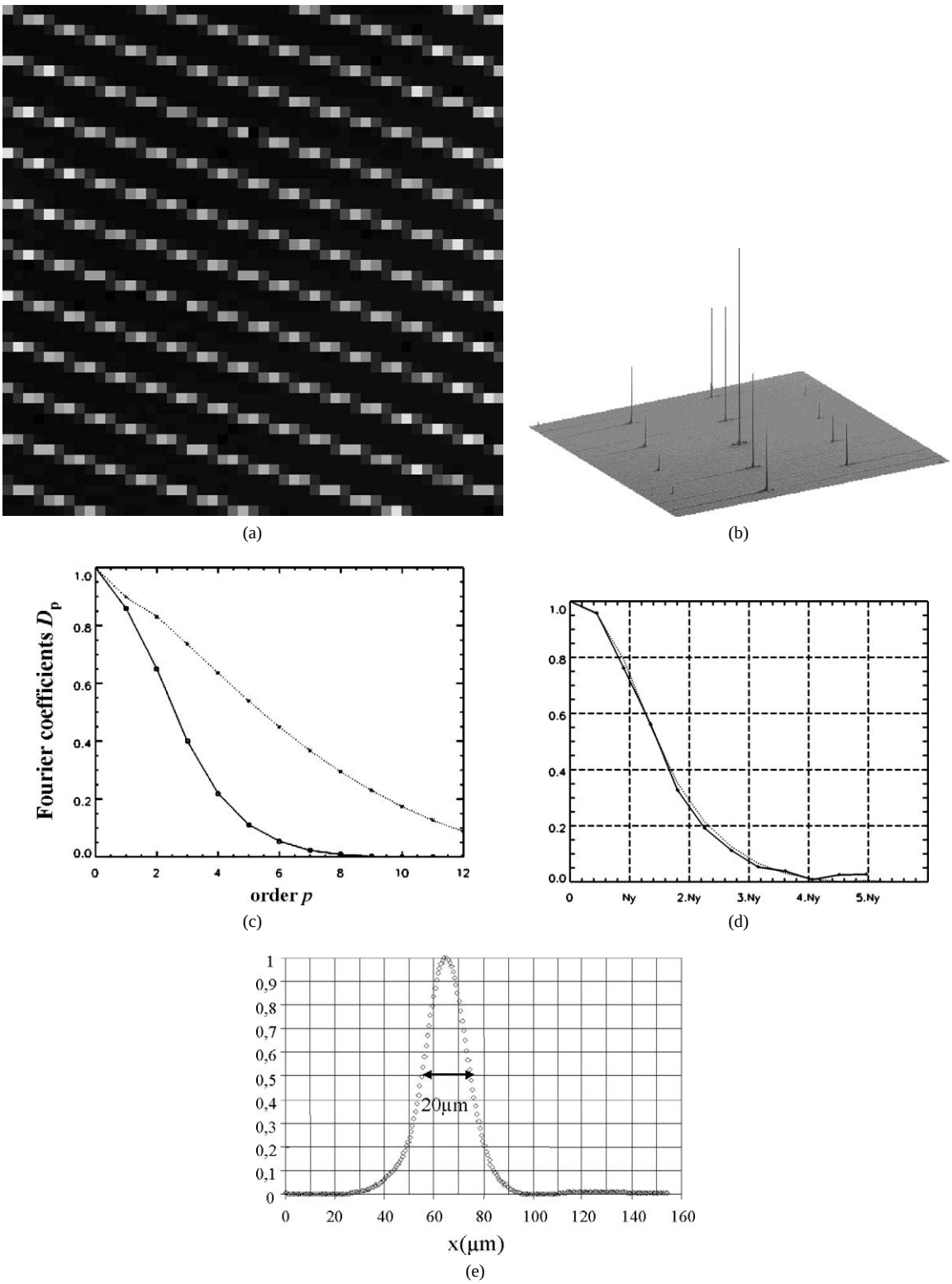

Fig. 8. Extraction of a mean LSF from (a) one image (50 by 50 pixels are represented); (b) by computing a 2D discrete Fourier transform; (c) the spatial frequencies extracted are compared to the predicted Fourier coefficients of the projected pattern; (d) leading to the pixel OTF; (e) an inverse FT of the OTF yields the mean LSF.

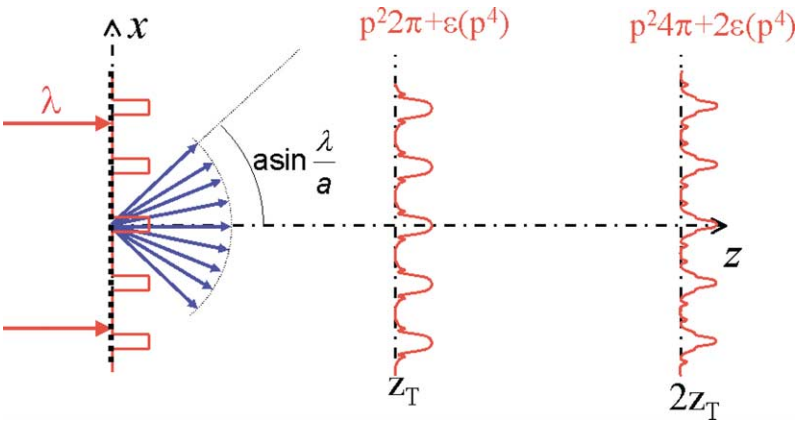

Fig. 9. Fundamental limitations in the monochromatic Talbot effect.

The 0-order propagates along the axis, and orders $-p$ and p are tilted with respect to the propagation axis by an angle θ_p given by the grating equation:

$$\sin\theta_p = \lambda p/d. \tag{1}$$

During their propagation, orders $-p$ and p are phase-delayed with respect to order 0, due to the slope of their wave vectors. This phase delay $\Delta\Phi_p$ is given by

$$\Delta\Phi_p(z) = \frac{2\pi}{\lambda} z[1-\cos\theta_p], \tag{2}$$

currently approximated by a parabolic relation:

$$\Delta\Phi_p(z) \approx 2\pi p^2 \frac{z}{z_T}, \tag{3}$$

where $z_T = 2d^2/\lambda$ is the Talbot distance.

At the Talbot distance, this phase delay is equal to $2\pi p^2$ for orders $+p$ and $-p$, and the initial state of interference is found. At half the Talbot distance, the phase delay is equal to πp^2, corresponding to a half period lateral translation.

If the slits width is close to the wavelength, the grating diffracts high orders and Eq. (3) is no longer valid for these orders. The high-angle diffracted orders no longer interfere constructively with the paraxial orders at the Talbot planes. When reducing the width a of the slits, these nonparaxial effects increase and the projected lines are more and more blurred in the Talbot planes [14]. Thus, at a given wavelength λ and for a grating period d, an optimal value of a must be found. For our application, a first numerical study has shown that one cannot project lines thinner than ∼35 μm using a grating of period 155 μm illuminated at $\lambda = 10$ μm [12].

As a consequence, new solutions have been investigated for measurements in the 8–12 μ spectral range.

3.4.2. Persisting Talbot patterns in polychromatic light

In his original experiment, Talbot used a Fraunhofer grating illuminated in polychromatic light and observed a regular alternation of numerous red and green coloured lines. Reconstituting this simple experiment, we have observed that at a certain distance from the grating, achromatic lines are formed whose transverse-resolution remains unaffected over a wide propagation-distance range [15]. Using a periodic object of period d in polychromatic illumination of spectral bandwidth $\Delta\lambda$, we demonstrated that this regime is reached at distance Z given by:

$$Z = \frac{2d^2}{\Delta\lambda}. \tag{4}$$

In the case of a binary amplitude mask of 1D periodicity, we established that the persisting Talbot pattern (PTP) generated can be written as an incoherent sum of fields produced by elementary cosinusoidal transmittances of period d/p. The intensity profile of the PTP generated by a grating of period d and slit width a is illustrated in Fig. 10. The PTP is periodic of period $d/2$ and the elementary cell is triangular of amplitude a/d and width $a/2$ at 50%. This result, demonstrated in the paraxial approximation domain, should remain true for periodic objects that diffract a large spectrum of orders. For our application, it should be possible to project high-resolution lines (or spots) in polychromatic light using a grating made of thin slits. This

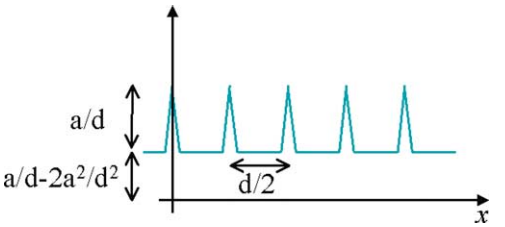

Fig. 10. Intensity profile of the persisting Talbot pattern produced by a 1D binary-amplitude grating of period d and slit width a.

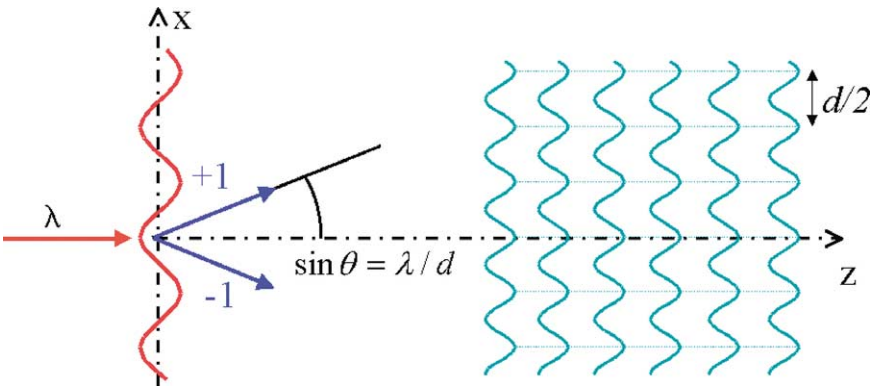

Fig. 11. Field generated by a continuously self-imaging grating. Simple example.

approach has to be validated. In particular, distance Z is dependant from the spectral bandwidth of the detector to be tested and must be reasonably high. Indeed, at a distance z from the grating, the image of the slit source of width w located at the entrance of the collimator is a line of width $w' = w \times z/f$, where f is the focal length of the collimator. For a high distance z, this image will enlarge the lines projected.

Another types of gratings have been explored in order to reduce this working distance Z.

3.4.3. Continuously self-imaging gratings

Let us consider an ideal transmittance of 1D periodicity that diffracts only two orders, $+1$ and -1. When illuminated by a plane wave, this ideal transmittance produces a field whose intensity profile is propagation- and wavelength-invariant (see Fig. 11). Indeed, at a wavelength λ, this field $E(x, z)$ can be written as the sum of two plane waves, that is:

$$E(x,z) = E_1\big[\exp(2\pi x \sin\theta_1/\lambda) + \exp(-2\pi x \sin\theta_1/\lambda)\big]\exp(2\pi z \cos\theta_1/\lambda). \tag{5}$$

The intensity pattern of $I(x,z) = |E(x,\underline{z})|^2$ is then given by:

$$I(x,z) = 4I_1 \cos^2(2\pi x/d), \tag{6}$$

an expression independent of z and λ.

Now, if we consider a periodic transmittance of 2D periodicity that diffracts plane waves whose wave vectors have the same slope with respect to the propagation axis, we obtain a field whose intensity pattern is a biperiodic array of achromatic and propagation-invariant bright spots. These fields are called non-diffracting arrays [16] and these biperiodic transmittances, the continuously self-imaging gratings [17]. On a practical level, a good approximation of these objects can be realised with a binary-phase grating. An example of the CSIG's approximation is illustrated in Fig. 12. For a given wavelength λ_0, this transmittance introduces a phase delay of π between the white and black areas of Fig. 12. At the other wavelengths λ, the phase delay is no longer π. The phase grating transmits a residual 0 order that interferes with the N orders ($N = 24$ in example of Fig. 12) diffracted by the CSIG and a residual Talbot distance appears at these wavelengths. In panchromatic light of spectral bandwidth $\Delta\lambda$, there is a distance Z' at which the achromatic and propagation-invariant regime is reached. This distance Z' is given by

$$Z' = 2a_0^2/\big(\eta^2 \Delta\lambda\big), \tag{7}$$

where a_0 is the period of the grating and η is a compression factor which is linked to the size r_0 of the projected spots [18]:

$$r_0 \approx 0.38 \times a_0/\eta. \tag{8}$$

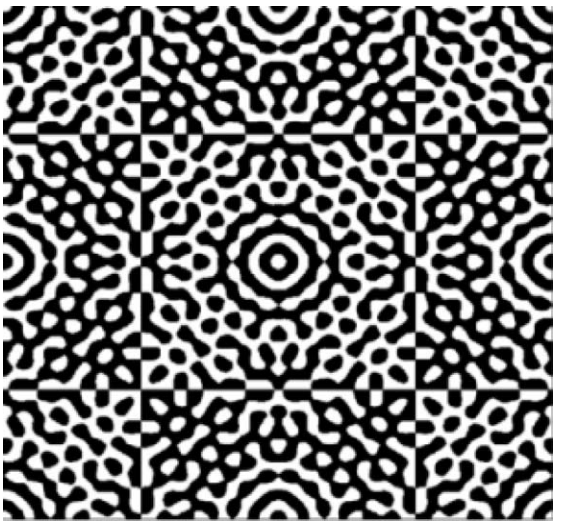

Fig. 12. Example of continuously self-imaging grating (two-level approximation).

For our application, it should be possible to project high-resolution in polychromatic light using a two-level approximation of a CSIG. Encouraging results have been obtained recently on an IRFPA of 320×240 microbolometers of pitch 35 μm, using a phase mask of pitch 1000 μm and of compression factor $\eta \approx 25.5$ [19].

3.4.4. Towards a universal test bench

In the first version of this test bench, the target – a Fraunhofer grating – was mounted in the cold shield directly in front of the sensor and was illuminated in quasi-monochromatic light. In a recent version, a phase grating illuminated in polychromatic light has been placed in front of a microbolometer array. Above a small distance (a few millimetres), this grating generates an array of achromatic and high-resolution spots with no need of precise focusing procedures. This first approach has offered new theoretical and practical tools, useful in developing a generic test bench conceived for measuring the spatial responses of any IRFPA (working in the small, medium or long infrared spectral range) and based on the use of self-imaging targets.

4. Conclusion

In this paper, new techniques of characterisation developed in our laboratory have been presented, allowing the measurement of the spatial and spectral responses of hundreds of thousands of pixels forming an infrared focal plane array. For the spectral assessments, a commercial FTIR spectrometer has been used to extract the hyperspectral cartographies of the IRFPA. An example of the measurement obtained with a large-format FPA of quantum-well technology has been presented. This test bench should be useful for technology engineers to understand and quantify the optical phenomena responsible for spectral nonuniformity.

For the spatial assessments, original Fourier-transform techniques have been proposed, based on the use of periodic targets whose details are sub-pixel. The projection of these high-resolution patterns that cover the entire sensor is provided by self-imaging objects illuminated by a polychromatic and collimated beam. This technique of projection requires no specific optics, except a commercial collimator and binary-amplitude or binary-phase gratings, that are compatible with the modern techniques of photolithography. The self-imaging phenomenon has been used in many areas of optics research [20], and its application to the metrology of IRFPAs could give rise to new concepts of infrared instruments, like micro-cameras, micro-spectrometers or micro-sensors of wavefronts.

Acknowledgements

The authors are grateful to J. Deschamps and E. Rosencher for their interest in this work.

References

[1] G.C. Holst, in: M.C. Dudzik (Ed.), The Infrared and Electro-Optical Systems Handbook, Vol. 4, Environmental Research Institute of Michigan, Ann Arbor, 1993, p. 203.
[2] D.G. Crowe, P.R. Norton, T. Limperis, J. Mudar, in: W.D. Rogatto (Ed.), The Infrared and Electro-Optical Systems Handbook, Vol. 3, Environmental Research Institute of Michigan, Ann Arbor, 1993, p. 237.
[3] R.J. Bell, Introductory Fourier Transform Spectroscopy, Academic Press, London, 1972.
[4] E. Costard, P. Bois, C. R. Physique 4 (2003).
[5] A. De Rossi, N. Guérineau, S. Rommeluere, E. Costard, Effect of finite pixel size on optical coupling in QWIPs, Infrared Phys. Technol., in press.
[6] R.F. Rauchmiller, R.A. Schowengerdt, Measurement of the Landsat Thematic Mapper modulation transfer function using an array of point sources, Opt. Engrg. 27 (1998) 334.
[7] J.W. Coltman, The specification of imaging properties by response to a sine wave input, J. Opt. Soc. Am. 44 (1954) 468.
[8] M. Chambon, J. Primot, M. Girard, Modulation transfer function assessment for sampled imaging systems: application of the generalized line spread function to a standard infrared camera, Infrared Phys. Technol. 37 (1996) 619.
[9] N. Guérineau, J. Primot, M. Tauvy, M. Caes, Modulation transfer function measurement of an infrared focal plane array using the self-imaging property of a canted periodic target, Appl. Opt. 38 (1999) 631.
[10] H.F. Talbot, Facts relating to optical science. No IV, Phil. Mag. 9 (1836) 401.
[11] J. Primot, M. Chambon, M. Caes, J. Deschamps, Evaluation of the modulation transfer function of an infrared focal plane array using the Talbot effect, J. Mod. Opt. 43 (1996) 347.
[12] N. Guérineau, Application du phénomène d'auto-imagerie à la caracterisation des matrices de détecteurs infrarouge, Thèse de l'Université Paris XI, Orsay, 1999.
[13] N. Guérineau, J. Primot, M. Caes, M. Tauvy, J. Deschamps, Experimental evaluation of the modulation transfer function of an infrared focal plane array using the Talbot effect, in: G.A. Lampropoulos, R.A. Lessard (Eds.), Proc. SPIE, Vol. 3491, 1998, p. 826.
[14] P.M. Mejias, R. Martinez Herrero, Diffraction by one-dimensional Ronchi grids: on the validity of the Talbot effect, J. Opt. Soc. Am. A 8 (1991) 266.
[15] N. Guérineau, B. Harchaoui, J. Primot, Talbot experiment re-examined: demonstration of an achromatic and continuous self-imaging regime, Opt. Commun. 180 (2000) 199.
[16] J. Primot, N. Guérineau, Non-diffracting arrays: theory, setups and applications, Recent Res. Devel. Opt. 2 (2002) 19.
[17] N. Guérineau, B. Harchaoui, J. Primot, K. Heggarty, Generation of achromatic and propagation-invariant spot arrays by use of continuously self-imaging gratings, Opt. Lett. 26 (2001) 411.
[18] N. Guérineau, J. Primot, Nondiffracting array generation using an N-wave interferometer, J. Opt. Soc. Am. A 16 (1999) 293.
[19] E. Di Mambro, N. Guérineau, J. Primot, Modulation transfer function measurement of an infrared focal plane array using a continuously self-imaging grating, in: G.C. Holst (Ed.), Proc. SPIE, Vol. 5076, 2003, in press.
[20] K. Patorski, The self-imaging phenomenon and its applications, in: E. Wolf (Ed.), Progress in Optics, Vol. 27, Elsevier, Amsterdam, 1989, pp. 1–108.